A Journal of the Gesellschaft Deutscher Chemiker

Angewandte International Edition GDCh Chemie

www.angewandte.org

Accepted Article

Title: Concerted bimetallic nanocluster synthesis and encapsulation via induced zeolite framework demetallation for shape and substrate selective heterogeneous catalysis

Authors: Takayuki Iida, Daniela Zanchet, Koji Ohara, Toru Wakihara, and Yuriy Román-Leshkov

To be cited as: *Angew. Chem. Int. Ed.* 10.1002/anie.201800557
Angew. Chem. 10.1002/ange.201800557

Link to VoR: http://dx.doi.org/10.1002/anie.201800557
http://dx.doi.org/10.1002/ange.201800557

WILEY-VCH

10.1002/anie.201800557

WILEY-VCH

Concerted bimetallic nanocluster synthesis and encapsulation via induced zeolite framework demetallation for shape and substrate selective heterogeneous catalysis

Takayuki Iida[a,b], Daniela Zanchet[b,c], Koji Ohara[d], Toru Wakihara[a]*, and Yuriy Román-Leshkov[b]*

Abstract: Bimetallic nanoparticle encapsulation in microporous zeolite crystals is a promising route for producing catalysts with unprecedented reaction selectivities. In this work, a novel synthetic approach was developed to produce $PtZn_x$ nanoclusters encapsulated inside zeolite micropores by introducing Pt^{2+} cations into a zincosilicate framework via ion exchange, followed by controlled demetallation and alloying with framework Zn. The resulting zeolites featured nanoclusters with sizes ~1 nm, having an interatomic structure corresponding to a $PtZn_x$ alloy as confirmed by pair distribution function (PDF) analysis. These materials featured simultaneous shape and substrate specificity demonstrated by the selective production of *p*-chloroaniline from the competitive hydrogenation of *p*-chloronitrobenzene and 1,3-dimethyl-5-nitrobenzene.

Nanocluster encapsulation inside zeolites is a powerful method for creating materials with unprecedented catalytic properties for many important reactions[1]. Encapsulation within micropores decreases nanoparticle sintering and elicits shape selectivity[2], both of which are difficult to implement with non-porous supports[3]. In recent years, several new synthetic routes have emerged for this purpose[4], including the introduction of stabilized metal species during zeolite crystallization[3,5], interzeolite phase transformation[6], coverage with zeolitic shells[7], and the inclusion of the metallic species in swollen two-dimensional zeolite precursors[8].

Bimetallic nanoclusters offer various properties that are unattainable by their monometallic counterparts[9]. The addition of a secondary metallic element induces changes in the electronic density of states (ligand effect)[10], and/or decreases the number of multiple-fold adsorption sites by partially blocking the surface (ensemble effect)[11]. These changes influence the substrate adsorption properties on the catalyst surface, resulting in unique catalytic consequences. Bimetallic catalysts have shown superior performances in the chemoselective reduction of alkynes to alkenes[12], conversion of Ŭ,ƀ-unsaturated aldehydes to allylic alcohols[13], and selective oxidation of CO to CO_2 in the presence of excess hydrogen[14]. To date, although some methods for bimetallic nanoparticle encapsulation have been reported[15], no facile methods exist to synthesize encapsulated bimetallic particles with base metals (which are prone to dissolve under zeolite synthesis conditions). Major limitations also include the formation of large nanoparticles outside of the zeolite crystals[16] and a lack of robust characterization tools to confirm the structure of nanoclusters with sizes < 1 nm. For these reasons, most efforts have focused on the encapsulation of monometallic nanoparticles. Indeed, the development of a simple method for encapsulating bimetallic nanoparticles inside zeolites is critical to generate improved heterogeneous catalysts with high specificity.

Here, we present an alternative strategy to generate bimetallic nanoparticles encapsulated within zeolite pores that overcomes the major synthetic bottlenecks described above (see Scheme 1). First, a Zn-containing MFI zeolite (Zn-MFI) was prepared via hydrothermal synthesis. After calcination, Pt^{2+} ions were exchanged into Zn-MFI to produce Pt^{2+}/Zn-MFI, taking advantage of the charge imbalance generated by the Zn in the framework. Lastly, sequential temperature-programmed calcination and reduction treatments were used for the one-step demetallation of Zn framework atoms and alloying with Pt species to generate composition-specific $PtZn_x$ bimetallic nanoclusters encapsulated in the pores of the MFI zeolite (denoted PtZn@MFI). Pair distribution function (PDF) analysis was used to understand the structural composition of the nanoclusters. Encapsulation of $PtZn_x$ nanoclusters was reflected in the highly shape- and chemoselective nature of the catalyst. Overall, this study shows that ion-exchange coupled with selective demetallation can be exploited as a powerful method to generate fully encapsulated bimetallic nanoclusters with exquisite compositional control.

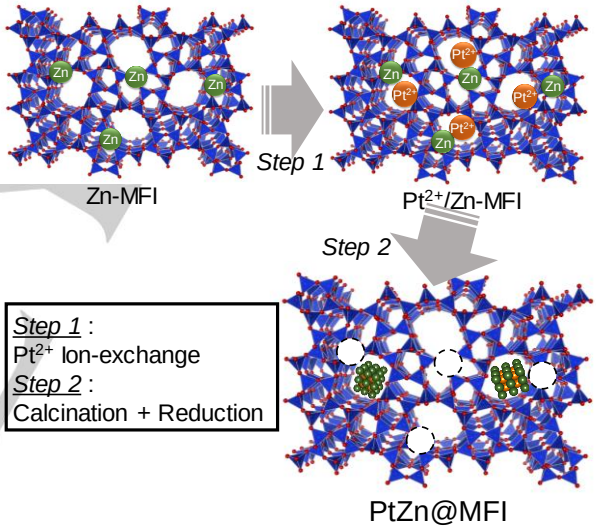

Scheme 1. Overall schematic of the synthesis route for PtZn@MFI. Step 1: Pt^{2+} is ion-exchanged into Zn-containing MFI zeolite; Step 2: calcination and subsequent reduction forms $PtZn_x$ bimetallic clusters inside the zeolite micropores. White dotted circles in PtZn@MFI represent the vacant silanol nests where framework Zn demetallation occurred.

The key strategy behind the formation of PtZn@MFI catalyst is the controlled demetallation of framework Zn while preserving the zeolite framework itself. Powder X-ray diffraction (PXRD) peaks corresponding to the MFI structure were confirmed in Zn-MFI and PtZn@MFI (Figure 1a); yet, the (111) diffraction peaks at 2ơ = 39.7º and 40.8° corresponding to metallic Pt or PtZn bulk phases, respectively, were not observed (Figure 1a inset, as confirmed by comparison with Pt and PtZn supported on silica). Inductively coupled plasma mass spectrometry (ICP-MS) analysis confirmed molar ratios of Si/Zn = 58 and Si/Pt = 320 in the PtZn@MFI (corresponding to Zn 1.8 wt% and Pt 0.98 wt%, respectively (Table S1)).

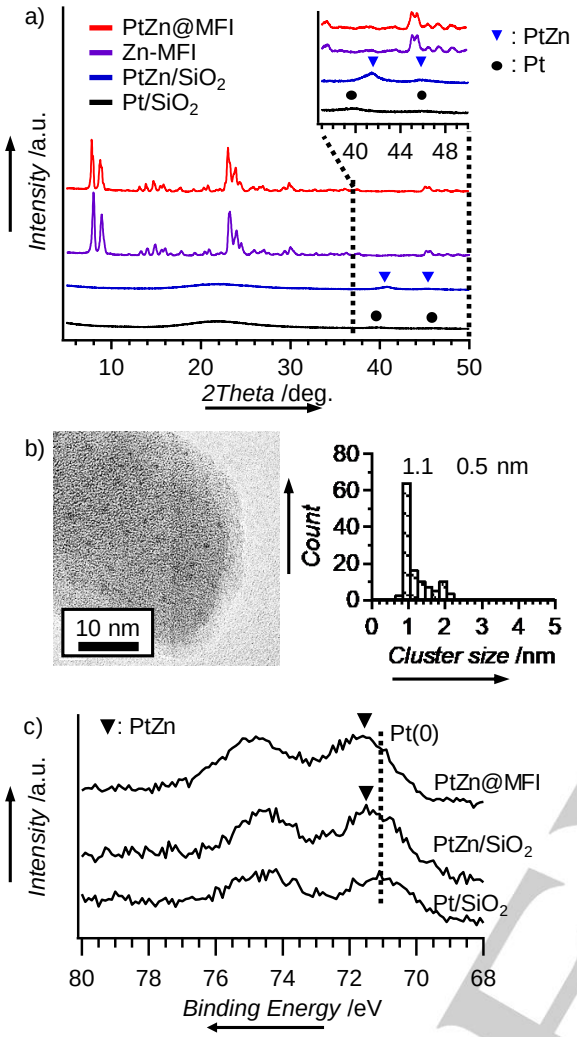

Figure 1. Catalysts characterization: a) PXRD patterns of Zn-MFI, PtZn@MFI, Pt/SiO_2 and $PtZn/SiO_2$. The region between 2ɗ = 37 to 50Å where (111) and (200) diffraction peaks of Pt and PtZn phases are present, is magnified in the inset. b) A representative TEM image of PtZn@MFI and corresponding size distribution. c) XPS spectra of PtZn@MFI, $PtZn/SiO_2$, and Pt/SiO_2. Carbon 1s spectra at 284.8 eV (assigned to adventitious carbon) was used as a calibration standard for all samples. Influence of charging on the energy shift was ruled out by confirming the peak position for Si 2p spectra at 103.5 eV (SiO_2).

Transmission electron microscopy (TEM) images confirmed that nanoparticles with average diameters ca. 1.1 nm were well dispersed in the zeolite crystals (Figure 1b). For comparison, a Pt@Al-MFI sample in which Pt clusters were encapsulated in an aluminosilicate MFI was prepared (see synthesis details in the ESI) with an identical Pt loading (~1 wt%). The particle size distribution in PtZn@MFI was similar to that found in Pt@Al-MFI (Figure S1), confirming that the particle size is determined by the framework structure for both cases. X-ray photoelectron spectroscopy (XPS) measurements showed a significant shift in the Pt $4f_{7/2}$ electron binding energy, suggesting the formation of an alloyed structure with zinc (Figure 1c). Although XPS is known as a surface specific technique, the penetration depth of Pt 4f electrons is about 7.5 nm (calculation details in ESI), and thus the results reflect the information of nanoclusters both on the surface and within the pores close to the surface of the zeolite crystal. Specifically, the positions of the Pt $4f_{7/2}$ peaks for PtZn@MFI and $PtZn/SiO_2$ were at 71.4 eV and 71.6 eV, respectively, both having larger binding energy values in comparison to Pt/SiO_2 (71.1 eV). We posit that alloying of Zn with Pt enhances the electrostatic field around the Pt nuclei[17], with depletion of Pt 5d density of states near the Fermi level and redistribution of charge involving (6s,6p) electrons, which causes a binding energy shift of the Pt 4f core levels to higher energies, and ultimately confirms alloy formation[18]. Ammonia temperature programmed desorption (NH_3-TPD) confirmed that the number of acid sites present in Zn-MFI decreased substantially after the formation of the bimetallic clusters (Figure S2). This result is in contrast to that obtained when using an aluminosilicate framework, wherein the acid site concentration was retained after heat treatment[19]. As such, the heating/reduction treatment performed in the second step of Scheme 1 is able to remove framework Zn atoms generating a material with a decreased number of acid sites, but fails to remove Al sites from the framework of the aluminosilicate zeolites.

The interatomic structure of the encapsulated metallic nanoclusters was investigated using differential pair distribution function (d-PDF) analysis (Figure 2). The d-PDF analysis is a method based on the difference of the PDFs, $G(r)$, of two components and can be used for obtaining structural information of materials with low crystallinity even in the presence of a known secondary crystalline phase[20]. In our case, given that eq. (1) is linear, the structure of a putative $PtZn_x$ alloy inside the MFI zeolite can be extrapolated assuming A is $PtZn_x$, B is MFI, A+B is PtZn@MFI, and x_A and x_B are coefficients. The d-PDF corresponds to the calculated difference in the experimental PDFs at the right side of eq. (1)ǫ in this case depicting the structure of $PtZn_x$ phase.

$$G_{A+B}(r) \cong x_A G_A(r) + x_B G_B(r) \cdots (1)$$
$$x_A G_A(r) \cong G_{A+B}(r) - x_B G_B(r) \cdots (1)'$$

The experimental PDFs of PtZn@MFI and Zn-MFI after acid treatment to remove Zn species (denoted as DeZn-MFI) are summarized in Figure 2a and the d-PDF of $PtZn_x$ is shown in Figure 2b. DeZn-MFI was used as a reference for this calculation since the absence of most framework Zn species in PtZn@MFI was confirmed by NH_3-TPD, and thereby such calculation would be effective in describing all the non-framework Pt and Zn species inside PtZn@MFI. The Faber-Ziman total structure factors, $S(Q)$, used for calculation of PDFs are summarized in Figure S3. The correlation peak positions of the d-PDF (Figure 2b) and the theoretical PDFs of bulk $PtZn_x$ alloys with different Pt:Zn ratios were calculated using the PDFgui software[21]. Figure 2c shows that the structure of the $PtZn_x$ species did not match with the Pt phase, but rather matched the $PtZn_x$ alloy references, thereby confirming $PtZn_x$ alloy formation. The structure corresponding to $PtZn_x$ (x = 1) alloy seemed to best account for the structure of the $PtZn_x$ clusters encapsulated in the zeolite (corresponding correlations shown as black dotted lines in Figures 2b and c). The strong correlations observed at r = 2.0 and 3.3 Å (shown with an asterisk in Figures 2b,e were assigned to **M-O** and **M**-O-**M**

correlations, respectively, with **M** corresponding to either Pt or Zn, since correlations at these distances were present both in bulk PtO_x (x = 1 and 2) and in ZnO phases (Figure S4). These data include both the **Zn**-O-**Zn** bonding of residual extraframework ZnO_x and the **Pt**-O-**Zn** bonding present at the surface-oxidized layer of the bimetallic clusters. The correlations for PtZn in PtZn@MFI were not confirmed at longer distances (*r* > 6 Å) (red dotted lines in Figures 2b and 2c). To verify that the low Pt weight loading was not the reason for the limited signal-to-noise (S/N) ratio observed, we performed d-PDF analysis on a control Pt@Al-MFI sample (Figure 2d and e, and S5). A d-PDF corresponding to a pure Pt phase was clearly observed, thereby confirming that if a Pt nanocluster had formed in our PtZn@MFI sample, it should have been visible in the d-PDF results. Thus, the reason for the low S/N ratio was assigned to the limited structural ordering of the $PtZn_x$ nanoclusters inside the zeolite.

The PtZn@MFI catalyst featured superb shape and substrate selective features as demonstrated by the simultaneous hydrogenation of *p*-chloronitrobenzene (ClNB) and 1,3-dimethyl-5-nitrobenzene (DMNB). The nitro groups in ClNB were targeted for reduction to produce *p*-chloroaniline (ClA) while also preventing both the hydrogenolysis of the C-Cl bond and the reduction of DMNBð a bulkier substrate that cannot diffuse into the MFI frameworkð to 1,3-dimethyl-5-aniline (DMA) (Figure 3a).

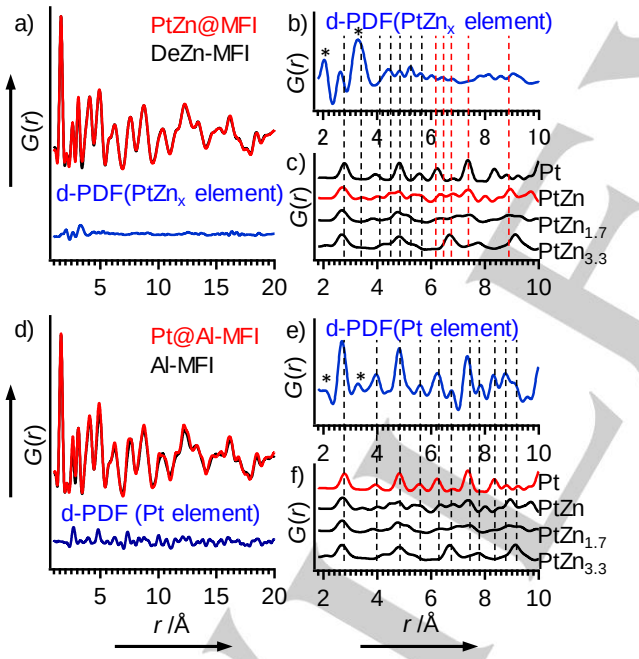

Figure 2. a) PDFs of PtZn@MFI and DeZn-MFI, and the calculated d-PDF of occluded $PtZn_x$ nanoclusters, b) magnification of the $PtZn_x$ d-PDF, c) simulated PDFs of $PtZn_x$ bimetallic alloys with different Pt:Zn ratios, d) PDFs of Pt@Al-MFI and Al-MFI, and the calculated d-PDF of occluded Pt nanoclusters, e) magnification of Pt d-PDF, and f) simulated PDFs of $PtZn_x$ bimetallic alloys with different Pt:Zn ratios (identical to c)). In c) and f), the most accountable structure for each case is highlighted in red, based on the comparison of the peak positions observed in the d-PDF and the theoretical PDF results. Correlations from **M**-**O**, **M**-O-**M** (**M** = Pt or Zn) present as extraframework ZnO_x or as a thin surface oxide layer of the nanoclusters are marked with asterisks (*).

On the one hand, the encapsulated bimetallic PtZn clusters featured a high substrate selectivity for the hydrogenation of ClNB to ClA that could not be achieved with the monometallic Pt controls. Specifically, PtZn@MFI achieved a selectivity of 83% at a conversion of 67% (Figure 3b). At the initial stage of the reaction the molar balance slightly decreased for this catalyst (Figure S6), eventually leveling off and resulting in improved selectivity at higher conversion values. In contrast, the Pt/SiO_2 control showed decreasing selectivity with increasing conversion (selectivity <60% at conversions >55%, Figure 3b), in agreement with the work by Coq[22] and Iihama[23], and generating significant irregularities in the carbon balance. Importantly, the hydrogenation of ClNB using a $PtZn/SiO_2$ control featured a selectivity of 91% at conversion of 64%, thus confirming that a PtZn bimetallic structure is needed to achieve high ClA selectivity.

On the other hand, the PtZn@MFI possessed shape selectivity features that could not be matched by non-microporous controls. This was demonstrated by comparing the resulting ClA/DMA molar yield ratio in the absence of external and internal diffusion limitations (Figure 3c, Table S2-S6 and Figure S7). The $PtZn/SiO_2$ control catalyst generated a ClA/DMA molar yield ratio below 5, in stark contrast to the value of 16 obtained with the PtZn@MFI catalyst after 40 min of reaction. To further enhance the substrate specificity of our catalyst, a chemical liquid deposition (CLD) treatment was performed before the calcination/reduction step (denoted as PtZn@MFI_CLD, structural characterization in Figure S8). This treatment added an amorphous silica layer around the zeolite crystal that has been shown to enhance the shape selectivity of zeolite catalysts[24]. Under identical reaction conditions, the PtZn@MFI_CLD catalyst showed similar performance in terms of selectivity and conversion (Figure 3b) to that of the PtZn@MFI parent material, but generated a significantly higher ClA/DMA molar yield ratio of 31 (Figure 3c). When comparing the catalytic results at high conversion values (~ 65%), the superb substrate-specific selectivity of the encapsulated catalysts can be clearly observed (see Table 1), and taken together, these data demonstrate that the CLD treatment had an additional beneficial effect on the shape selectivity. Since DMNB is too large to enter the MFI micropores[25], we hypothesize that the CLD treatment effectively passivated any $PtZn_x$ clusters on the external surface of the zeolite crystals and/or prevented small metallic clusters near the surface to diffuse out of the pores. In complement to the TEM observations, which show size distributions commensurate with encapsulation but cannot differentiate between the location of the clusters, the results of the control reaction using DMNB provide a strong evidence for successful encapsulation of bimetallic nanoclusters within the zeolite pores. Finally, a control experiment with Pt@Al-MFI catalyst did not generate observable amounts of hydrogenation products, presumably due to formation of oligomeric byproducts that coke the pores (Figure S9). In this respect, the capability to remove the acid sites is beneficial for the reactions displayed herein, and presents yet another advantage of our synthetic method.

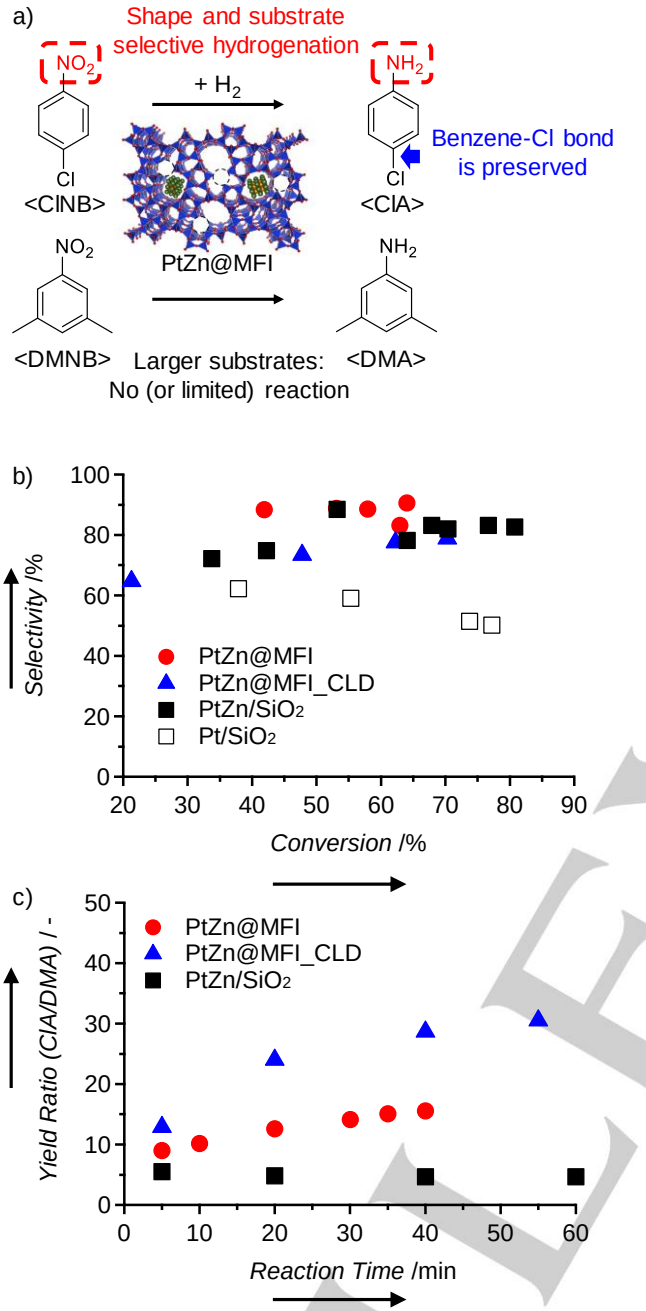

Figure 3. a) Reaction scheme for the shape and substrate selective hydrogenation of *p*-chloronitrobenzene (ClNB) to *p*-chloroaniline (ClA) in the presence of 1,3-dimethyl-5-nitrobenzene (DMNB). The abbreviation for each substance is written in < >. b) Conversion-selectivity plot of ClNB to ClA on PtZn@MFI, PtZn@MFI_CLD, PtZn/SiO_2, and Pt/SiO_2 catalysts. c) Time profile of the molar ratio of the yield for ClA and DMA on PtZn@MFI, PtZn@MFI_CLD, and PtZn/SiO_2 catalysts. Reaction conditions: Substrate (ClNB and DMNB): 0.2 mmol in 10 mL of heptane; reaction temperature: 70°C; stirring speed: 800 rpm; H_2 pressure: 1 atm; catalyst loading: 200 mg (PtZn@MFI), 250 mg (PtZn@MFI_CLD), 50 mg (PtZn/SiO_2), 15 mg (Pt/SiO_2). The hydrogenation using Pt/SiO_2 catalyst was performed in the absence of DMNB to confirm the activity of this catalyst only in the presence of ClNB and hydrogen.

Table 1. Conversion values for ClNB and DMNB and the yields to ClA and DMA during the competitive hydrogenation experiments at ~65% ClNB conversion. Reaction conditions identical to those described in Figure 3.

	Conversion [%] (ClNB)	Yield [%] (ClA)	Conversion [%] (DMNB)	Yield [%] (DMA)
PtZn@MFI_CLD	62	48	2.6	1.7
PtZn@MFI	68	56	6.0	3.7
PtZn/SiO_2	64	58	14	13

In summary, we developed a versatile method to encapsulate PtZn bimetallic nanoclusters inside the pores of MFI zeolites, generating catalysts with excellent shape selectivity and substrate specificity. Recently, incorporation of monometallic nanoparticles inside the zeolite micropores was shown to drastically change reaction selectivity.[7a] For the present system, we know that on the one hand, PtZn nanoclusters are needed to achieve high hydrogenation selectivity of halogenated nitroarene compounds; and on the other hand, that microporous materials are needed to achieve size selectivity in the presence of two nitroarene substrates of different sizes. The main bottleneck involves the lack of facile methods to generate bimetallic nanoclusters (e.g., PtZn) within zeolite micropores. This limitation is due to the challenging nature of placing (bi)metallic nanoclusters of uniform composition inside the pores. Indeed, most methods follow sequential impregnation approaches which result in highly heterogeneous mixtures of metal precursors, ultimately leading to non-uniformity in the bimetallic cluster composition. Our method exploits the selective demetallation of framework Zn atoms to alloy with Pt^{2+} cations in a controlled fashion to produce targeted bimetallic nanoclusters. The catalyst was able to selectively reduce the nitro groups in *p*-chloronitrobenzene, in the presence of 1,3-dimethyl-5-nitrobenzene, a bulkier substrate, exemplifying simultaneous substrate and shape selectivity. The synthesis route can be easily extended to different metals, and represents a straightforward methodology for preparing bimetallic nanoclusters encapsulated inside zeolites that are essential for next-generation catalysis.

Acknowledgements

This work was supported by the U.S. Department of Energy, Office of Basic Energy Sciences under Award No. DE-SC0016214. The High Energy Total X-ray Scattering experiments conducted at SPring-8 were approved by the Japan Synchrotron Radiation Research Institute (Proposal Nos. 2016B0115 and 2017A0115). T. I. thanks the Japan Society for the Promotion of Science for a Grant-in-aid for Scientific research, supported by JSPS KAKENHI Grant Number 15J07161, and the Program for Leading Graduate Schools, ñGlobal Leader Program for Social Design and Management (GSDM)ò by the Ministry of Education, Culture, Sports, Science and Technology, for the financial support. D. Z. acknowledges funding by the São Paulo Research Foundation (FAPESP

2015/23900-2) and the National Council of Technological and Scientific Development (CNPq 309373/2014-0).

Keywords: Alloys, Bimetallic, Encapsulation, Heterogeneous catalysis, Zeolites

[1] a) A. Corma, P. Concepcion, M. Boronat, M. J. Sabater, J. Navas, M. J. Yacaman, E. Larios, A. Posadas, M. A. Lopez-Quintela, D. Buceta, et al., *Nat. Chem.* **2013**, *5*, 775ï 781; b) M. Flytzani-Stephanopoulos, B. C. Gates, *Annu. Rev. Chem. Biomol. Eng.* **2012**, *3*, 545ï 574.

[2] A. B. Laursen, K. T. Hojholt, L. F. Lundegaard, S. B. Simonsen, S. Helveg, F. Schuth, M. Paul, J. D. Grunwaldt, S. Kegnoes, C. H. Christensen, et al., *Angew. Chem. Int. Ed.* **2010**, *49*, 3504ï 3507.

[3] J. L. Lu, B. S. Fu, M. C. Kung, G. M. Xiao, J. W. Elam, H. H. Kung, P. C. Stair, *Science* **2012**, *335*, 1205ï 1208.

[4] D. Farrusseng, A. Tuel, *New J. Chem.* **2016**, *40*, 3933ï 3949.

[5] a) M. Choi, Z. J. Wu, E. Iglesia, *J. Am. Chem. Soc.* **2010**, *132*, 9129ï 9137; b) S. Goel, Z. J. Wu, S. I. Zones, E. Iglesia, *J. Am. Chem. Soc.* **2012**, *134*, 17688ï 17695; c) N. Wang, Q. M. Sun, R. S. Bai, X. Li, G. Q. Guo, J. H. Yu, *J. Am. Chem. Soc.* **2016**, *138*, 7484ï 7487; d) M. Moliner, J. E. Gabay, C. E. Kliewer, R. T. Carr, J. Guzman, G. L. Casty, P. Serna, A. Corma, *J. Am. Chem. Soc.* **2016**, *138*, 15743ï 15750

[6] S. Goel, S. I. Zones, E. Iglesia, *J. Am. Chem. Soc.* **2014**, *136*, 15280ï 15290.

[7] a) J. Zhang, L. Wang, Y. Shao, Y. Wang, B. C. Gates, F.-S. Xiao, *Angew. Chem. Int. Ed.* **2017**, *56*, 9747ï 9751; b) S. W. Li, L. Burel, C. Aquino, A. Tuel, F. Morfin, J. L. Rousset, D. Farrusseng, *Chem. Commun.* **2013**, *49*, 8507ï 8509.

[8] a) L. C. Liu, U. Diaz, R. Arenal, G. Agostini, P. Concepcion, A. Corma, *Nat. Mater.* **2017**, *16*, 132ï 138. b) Z. Zhao, Y. Li, M. Feyen, R. McGuire, U. Müller, W. Zhang, *ChemCatChem* **2018**, DOI 10.1002/cctc.201800040.

[9] a) M. Armbrüster, R. Schlögl, Y. Grin, *Sci. Technol. Adv. Mater.* **2014**, *15*, 34803; b) S. Furukawa, T. Komatsu, *ACS Catal.* **2017**, *7*, 735ï 765.

[10] P. Liu, J. K. Norskov, *Phys. Chem. Chem. Phys.* **2001**, *3*, 3814ï 3818.

[11] F. Gao, D. W. Goodman, *Chem. Soc. Rev.* **2012**, *41*, 8009ï 8020.

[12] M. Armbruster, K. Kovnir, M. Friedrich, D. Teschner, G. Wowsnick, M. Hahne, P. Gille, L. Szentmiklosi, M. Feuerbacher, M. Heggen, et al., *Nat. Mater.* **2012**, *11*, 690ï 693.

[13] C. M. Li, Y. D. Chen, S. T. Zhang, S. M. Xu, J. Y. Zhou, F. Wang, M. Wei, D. G. Evans, X. Duan, *Chem. Mater.* **2013**, *25*, 3888ï 3896.

[14] C. X. Xiao, L. L. Wang, R. V Maligal-Ganesh, V. Smetana, H. Walen, P. A. Thiel, G. J. Miller, D. D. Johnson, W. Y. Huang, *J. Am. Chem. Soc.* **2013**, *135*, 9592ï 9595.

[15] a) S. W. Li, A. Tuel, J. L. Rousset, F. Morfin, M. Aouine, L. Burel, F. Meunier, D. Farrusseng, *ChemNanoMat* **2016**, *2*, 534ï 539; b) T. Otto, J. M. Ramallo-Lopez, L. J. Giovanetti, F. G. Requejo, S. I. Zones, E. Iglesia, *J. Catal.* **2016**, *342*, 125ï 137.

[16] a) T. Komatsu, H. Ikenaga, *J. Catal.* **2006**, *241*, 426ï 434; b) W. Huang, W. Pyrz, R. F. Lobo, J. G. Chen, *Appl. Catal. A Gen.* **2007**, *333*, 254ï 263.

[17] A. Naitabdi, R. Fagiewicz, A. Boucly, G. Olivieri, F. Bournel, H. Tissot, Y. W. Xu, R. Benbalagh, M. G. Silly, F. Sirotti, et al., *Top. Catal.* **2016**, *59*, 550ï 563.

[18] J. A. Rodriguez, M. Kuhn, *J. Chem. Phys.* **1995**, *102*, 4279ï 4289.

[19] A. Philippaerts, S. Paulussen, A. Breesch, S. Turner, O. I. Lebedev, G. Van Tendeloo, B. Sels, P. Jacobs, *Angew. Chem. Int. Ed.* **2011**, *50*, 3947ï 3949.

[20] J. Peterson, J. TenCate, T. Proffen, T. Darling, H. Nakotte, K. Page, *J. Appl. Crystallogr.* **2013**, *46*, 332ï 336.

[21] C. L. Farrow, P. Juhas, J. W. Liu, D. Bryndin, E. S. Boģin, J. Bloch, T. Proffen, S. J. L. Billinge, *J. Phys. Condens. Matter* **2007**, *19*, 335219.

[22] B. Coq, A. Tijani, F. Figueras, *J. Mol. Catal.* **1992**, *71*, 317ï 333.

[23] S. Iihama, S. Furukawa, T. Komatsu, *ACS Catal.* **2016**, *6*, 742ï 746.

[24] a) S. R. Zheng, H. R. Heydenrych, A. Jentys, J. A. Lercher, *J. Phys. Chem. B* **2002**, *106*, 9552ï 9558; b) Y. T. Cheng, Z. Wang, C. J. Gilbert, W. Fan, G. W. Huber, *Angew. Chem. Int. Ed.* **2012**, *51*, 11097ï 11100.

[25] V. R. Choudhary, V. S. Nayak, T. V Choudhary, *Ind. Eng. Chem. Res.* **1997**, *36*, 1812ï 1818.

10.1002/anie.201800557

WILEY-VCH

Entry for the Table of Contents (Please choose one layout)

Layout 1:

COMMUNICATION

A new method to produce $PtZn_x$ bimetallic nanoclusters encapsulated inside MFI zeolite crystals was developed by introducing Pt^{2+} cations into a zincosilicate framework via ion exchange, followed by controlled demetallation and reduction. The resulting zeolites featured $PtZn_x$ nanoclusters with sizes ~1 nm, possessing simultaneous shape and substrate specificity.

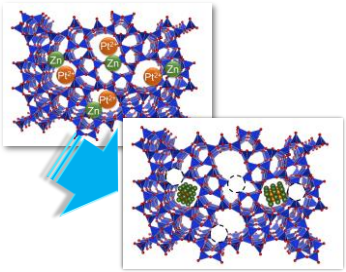

$PtZn_x$ nanoclusters encapsulated in zeolites from Pt^{2+} ion-exchanged zincosilicates

*Author(s), Corresponding Author(s)**

Page No. – Page No.

Title